Study of Lyman-α Polarization due to Anisotropic Electron Collisions in LHD*)

Nilam RAMAIYA[1)], Motoshi GOTO[1,2)], Tetsutarou OISHI[1,2)] and Shigeru MORITA[1,2)]

[1)]*Department of Fusion Science, SOKENDAI (The Graduate University for Advanced Studies), Toki 509-5292, Japan*
[2)]*National Institute for Fusion Science, Toki 509-5292, Japan*

(Received 9 January 2019 / Accepted 22 March 2019)

We have investigated the polarization of Lyman-α line in the Large Helical Device (LHD). A theoretical model has been developed for a quantitative understanding of the anisotropy in the electron velocity distribution function (EVDF). The present model treats an anisotropic EVDF having different electron temperatures in the directions parallel and perpendicular to the magnetic field. The steady-state time period of an electron cyclotron heated discharge has been analyzed and the comparison between the theoretical and measured polarization degrees suggests that in the edge plasma the difference between these two temperatures is approximately 10%. In addition, the dependence of the observed Lyman-α intensity on the angle of the linearly polarized light has been studied. The obtained results show that in the experimentally observed intensity the inboard side emission dominates over the emission from the outboard side and in the edge LHD plasma the electron temperature in the perpendicular direction to the magnetic field is higher than that in the parallel direction.

Keywords: Lyman-α line, velocity distribution function, polarization degree, VUV spectrometer, Large Helical Device

DOI: 10.1585/pfr.14.3402083

1. Introduction

The measurement of anisotropy in the electron velocity distribution function (EVDF) can provide significant information for understanding transport phenomena, equilibria, and current drive in a fusion plasma. Although the anisotropic EVDF plays an important role in a magnetically confined fusion plasma [1], it has not been actively investigated in plasma experiments. Plasma polarization spectroscopy can be a useful technique to study the anisotropy in the EVDF [2]. In the present study we deal with the polarization of Lyman-α line caused by anisotropic collisions with electrons.

The Large Helical Device (LHD) is a heliotron-type magnetic confinement fusion experimental device. The measurements of Lyman-α line polarization have been carried out in LHD. On the other hand, the development of a theoretical model is necessary to correlate the experimentally measured polarization and the anisotropy in the EVDF. This spectral line at 121.56 nm has been chosen for this purpose because, owing to the simple energy level structure relating to this line, development of an accurate theoretical model is possible.

The previous study regarding hydrogen emission in LHD suggests that the dominant emissions of hydrogen are located outside the confined region of the plasma [3,4], which consists of stochastic magnetic field lines. In such regions, the confinement characteristics of the electrons are strongly dependent on their velocity pitch angle with respect to the magnetic field direction. In LHD the strength of the magnetic field varies in the toroidal direction and because of that electrons move under the influence of a mirror effect. Electrons having a small pitch angle, known as passing electrons, can escape easily from the magnetic mirror but those with a large pitch angle, known as trapped electrons, are trapped inside the ripples of the magnetic field strength. As a result, the confinement time of trapped electrons should be longer than that of passing electrons, which would cause the anisotropy in the EVDF.

The theoretical framework for calculating the polarization of Lyman-α due to anisotropic electron collisions following the methodology proposed by Fujimoto [2] is described in Sec. 2 with some initial results. For a comparison of the model results with the measured results, some geometrical aspects of the measurements in LHD need to be taken into account. The details are described in Sec. 3 and the obtained results are shown in Sec. 4.1. In Sec. 4.2 the comparison between the variation of experimentally observed intensity and the simulated intensity with the angle of linearly polarized light is discussed.

2. Theoretical Model

The Lyman-α line consists of two components, i.e., $1\,^2S_{1/2} - 2\,^2P_{1/2}$ and $1\,^2S_{1/2} - 2\,^2P_{3/2}$. Figure 1 shows all the possible transitions among the magnetic sublevels relating to the Lyman-α line. As indicated in the figure,

author's e-mail: nilam.nimavat@nifs.ac.jp

*) This article is based on the presentation at the 27th International Toki Conference (ITC27) & the 13th Asia Pacific Plasma Theory Conference (APPTC2018).

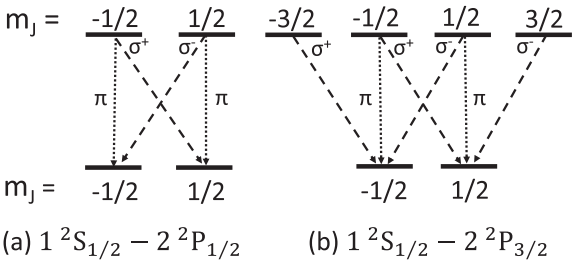

Fig. 1 Transitions among the magnetic sublevels relating to the Lyman-α line. The dashed and dotted lines indicate $\sigma-$light and $\pi-$light, respectively.

the $\Delta m_J = 0$ transition emits $\pi-$light, linearly polarized in the quantization axis direction, and $\Delta m_J = \pm 1$ transitions emit $\sigma-$light, circularly polarized in the plane perpendicular to the quantization axis. Here m_J means the magnetic quantum number of the level having the total angular momentum quantum number J. When all the magnetic sublevels are populated uniformly, the emitted light intensity is isotropic, i.e., the line is not polarized. However, the imbalance of the population among the sublevels results in the polarization of emitted light.

Here, the quantization axis is taken to be in the magnetic field direction. We assume an axisymmetric system with respect to the quantization axis where there is no orientation among the magnetic sublevels, i.e., the populations of m_J and $-m_J$ sublevels are the same. For this reason the emitted light corresponding to the $1\,^2S_{1/2} - 2\,^2P_{1/2}$ transition is not polarized, while the $1\,^2S_{1/2} - 2\,^2P_{3/2}$ transition may emit polarized light. For developing a theoretical model, first the $1\,^2S_{1/2} - 2\,^2P_{3/2}$ transition is considered and in the final result the influence of the unpolarized $1\,^2S_{1/2} - 2\,^2P_{1/2}$ transition is taken into account.

The assumptions above mentioned imply that for an axisymmetric system the density matrix of an excited state p, can be approximately expanded as [2]

$$\rho(p) = \rho_0^0(p)\, T_0^{(0)}(p) + \rho_0^2(p)\, T_0^{(2)}(p), \tag{1}$$

where $T_q^{(k)}(p)$ is the irreducible tensor operator [5]. The expansion coefficients $\rho_q^k(p)$ are given by [2]

$$\rho_q^k(p) = \sum_{MN} (-1)^{J-N} \langle JJM - N \,|\, kq \rangle \rho_{M,N}(p). \tag{2}$$

Here, $\langle JJM-N \,|\, kq\rangle$ is the Clebsch-Gordan coefficient and $\rho_{M,N}(p)$ is the elements of the density matrix in the $|J\ m_J\rangle$ representation. Thus, two quantities are assigned to each energy level: population $\rho_0^0(p)$ and alignment $\rho_0^2(p)$. The conventional population $n(p)$ is expressed by

$$n(p) = \sqrt{2J_p + 1}\,\rho_0^0(p). \tag{3}$$

The alignment is a measure of the population imbalance among the magnetic sublevels in a J level. Henceforth, for simplicity, $a(p)$ is used in place of $\rho_0^2(p)$.

Under the corona equilibrium, the population of the excited state p is balanced by the electron impact excitation from the ground state and the spontaneous radiative decay. The rate equation for the population can be given as

$$C^{0,0}(1, p)\, n_e\, n(1) = \sum_s A(p, s)\, n(p), \tag{4}$$

where $C^{0,0}(1, p)$ is the rate coefficient for the electron impact excitation, $A(p, s)$ is the Einstein A coefficient for the transition from a level p to a lower level s, and n_e is the electron density. Similarly, the rate equation for $a(p)$ can be expressed as

$$C^{0,2}(1, p)\, n_e\, n(1) = \sum_s A(p, s)\, a(p), \tag{5}$$

where $C^{0,2}(1, p)$ is the alignment creation rate coefficient. The population, $n(p)$, and the alignment, $a(p)$, are then derived as

$$n(p) = \frac{C^{0,0}(1, p)\, n_e}{\sum_s A(p, s)}\, n(1), \tag{6}$$

$$a(p) = \frac{C^{0,2}(1, p)\, n_e}{\sum_s A(p, s)}\, n(1). \tag{7}$$

We consider a case in which the emission line is observed from a direction perpendicular to the quantization axis, using a linear polarizer. The longitudinal alignment, A_L, is defined as [2]

$$A_L = \frac{I_\parallel - I_\perp}{I_\parallel + 2I_\perp}, \tag{8}$$

where $I_\parallel$ and $I_\perp$ are the linearly polarized light intensities in the direction parallel and perpendicular to the quantization axis, respectively. For a transition from a level p to a level s, A_L and the relative alignment $a(p)/n(p)$, are related as [2]

$$A_L(p, s) = (-1)^{J_p + J_s} \sqrt{\frac{3}{2}} (2J_p + 1) \times \begin{Bmatrix} J_p & J_p & 2 \\ 1 & 1 & J_s \end{Bmatrix} \frac{a(p)}{n(p)}, \tag{9}$$

where $\{\cdots\}$ is the 6-j symbol.

Calculations of the coefficients $C^{0,0}(1, p)$ and $C^{0,2}(1, p)$ are carried out under a certain EVDF. We assume that the EVDF is axisymmetric with respect to the quantization axis and the electron temperature has different values in the directions parallel and perpendicular to the quantization axis or the magnetic field. The explicit expression for such EVDFs is given as [2]

$$f(v, \theta) = 2\pi \left(\frac{m}{2\pi k}\right)^{\frac{3}{2}} \left(\frac{1}{T_\perp^2 T_\parallel}\right)^{\frac{1}{2}} \times \exp\left[- \frac{mv^2}{2k} \left(\frac{\sin^2\theta}{T_\perp} + \frac{\cos^2\theta}{T_\parallel} \right) \right], \tag{10}$$

where v is the absolute value of the velocity, θ is the pitch angle of the velocity with respect to the magnetic field, and

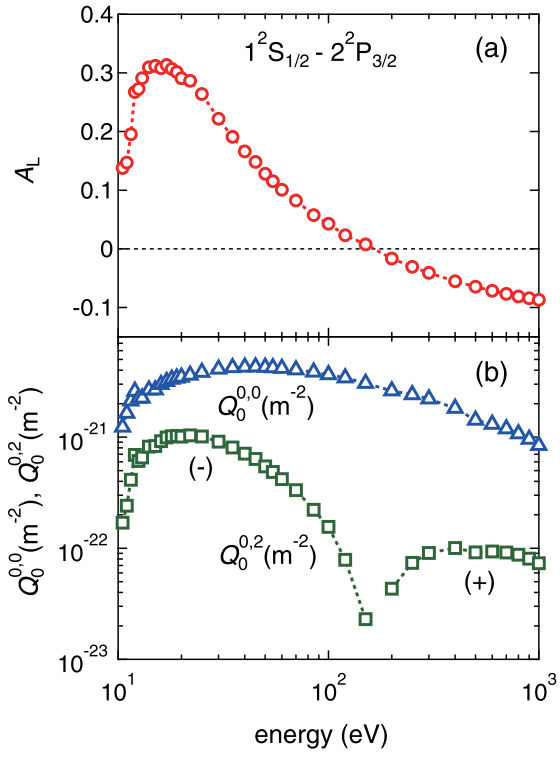

Fig. 2 (a) Longitudinal alignment, A_L, values under the condition that the hydrogen atoms are excited by a monoenergetic beam of electrons and (b) population creation cross section, $Q_0^{0,0}$, and alignment creation cross section, $Q_0^{0,2}$, for the $1\,^2S_{1/2} - 2\,^2P_{3/2}$ transition.

m and k are the electron mass and the Boltzmann constant, respectively. Here, $T_\parallel$ and $T_\perp$ represent the electron temperature in the directions parallel and perpendicular to the magnetic field, respectively.

The rate coefficients $C^{0,0}(1,p)$ and $C^{0,2}(1,p)$ are evaluated as [2]

$$C^{0,0}(1,p) = \int Q_0^{0,0}(1,p)\, 4\pi\, f_0(v)\, v^3\, \mathrm{d}v, \tag{11}$$

$$C^{0,2}(1,p) = \int Q_0^{0,2}(1,p)\, [4\pi\, f_2(v) / 5]\, v^3\, \mathrm{d}v, \tag{12}$$

where $Q_0^{0,0}(1,p)$ and $Q_0^{0,2}(1,p)$ are the excitation and alignment creation cross sections, respectively, for the corresponding transition, and $f_0(v)$ and $f_2(v)$ are the coefficients of expansion of $f(v,\theta)$ by the Legendre polynomials, $P_K(\cos\theta)$, as

$$f(v,\theta) = \sum_K f_K(v)\, P_K(\cos\theta). \tag{13}$$

The coefficient $f_K(v)$ is explicitly given as

$$f_K(v) = \frac{2K+1}{2} \int f(v,\theta)\, P_K(\cos\theta)\, \sin\theta\, \mathrm{d}\theta. \tag{14}$$

The alignment creation cross section $Q_0^{0,2}(1,p)$ is obtained from the $Q_0^{0,0}(1,p)$ as [2]

$$Q_0^{0,2}(1,p) = (-1)^{J_p+J_s} \sqrt{\frac{2}{3}}\, (2J_p+1)^{-1} \times \begin{Bmatrix} J_p & J_p & 2 \\ 1 & 1 & J_s \end{Bmatrix}^{-1} A_L(p,1)\, Q_0^{0,0}(1,p). \tag{15}$$

The data for $Q_0^{0,0}(1,p)$ and A_L are obtained from Refs. [6] and [7], respectively. Here, A_L is the value for the case where the hydrogen atoms are excited with a monoenergetic beam of electrons and the emitted Lyman-α radiation is observed from a direction perpendicular with respect to the incident electron beam axis. That means the observation angle is 90°. Figure 2 shows these quantities for the $1\,^2S_{1/2} - 2\,^2P_{3/2}$ transition.

The polarization degree for this transition, which may emit polarized radiation is defined as

$$P_1 = \frac{I_{\parallel 1} - I_{\perp 1}}{I_{\parallel 1} + I_{\perp 1}}, \tag{16}$$

where $I_{\parallel 1}$ and $I_{\perp 1}$ stand for the intensities in the parallel and perpendicular directions to the quantization axis, respectively.

The unpolarized transition, $1\,^2S_{1/2} - 2\,^2P_{1/2}$, is included in the observed line and its influence is evaluated. We assume that the $2\,^2P_{1/2}$ and $2\,^2P_{3/2}$ states are populated according to their statistical weight, i.e.,

$$n(2\,^2P_{1/2}) = \frac{1}{2}\, n(2\,^2P_{3/2}), \tag{17}$$

where $n(2\,^2P_{1/2})$ and $n(2\,^2P_{3/2})$ are the total populations of the states $2\,^2P_{1/2}$ and $2\,^2P_{3/2}$, respectively.

The resulting polarization degree, denoted here as P_{res}, which takes into account both the transitions is expressed as

$$P_{\mathrm{res}} = \frac{(I_{\parallel 1} + I_{\parallel 2}) - (I_{\perp 1} + I_{\perp 2})}{(I_{\parallel 1} + I_{\parallel 2}) + (I_{\perp 1} + I_{\perp 2})}. \tag{18}$$

Here, $I_{\parallel 2}$ and $I_{\perp 2}$ are the intensities of the $1\,^2S_{1/2} - 2\,^2P_{1/2}$ transition in the directions parallel and perpendicular to the quantization axis, respectively.

Because the $1\,^2S_{1/2} - 2\,^2P_{1/2}$ line is unpolarized, $I_{\parallel 2} = I_{\perp 2}$, and $I_{\parallel 2} + I_{\perp 2} = (I_{\parallel 1} + I_{\perp 1})/2$ from the assumption above, P_{res} is rewritten as

$$P_{\mathrm{res}} = \frac{I_{\parallel 1} - I_{\perp 1}}{(I_{\parallel 1} + I_{\perp 1}) + (I_{\parallel 2} + I_{\perp 2})} = \frac{2}{3} P_1. \tag{19}$$

The P_{res} evaluated for different $T_\parallel$ and $T_\perp$ values are shown in Fig. 3. The results indicate that the value of polarization is negative for $T_\perp > T_\parallel$ and is positive for $T_\perp < T_\parallel$.

3. Lyman-α Polarization for LHD Experiments

We define the "angle of observation" to be the angle between the line of sight and the quantization axis. For the

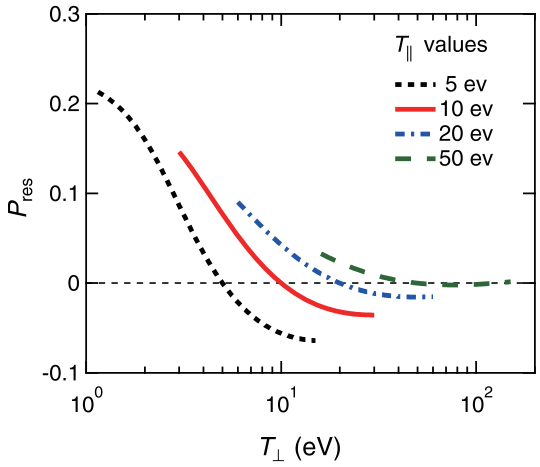

Fig. 3 Polarization degree calculated for different $T_\parallel$ and $T_\perp$ under the assumption of corona equilibrium. $T_\parallel$ and $T_\perp$ refer to the electron temperatures in the directions parallel and perpendicular to the magnetic field, respectively.

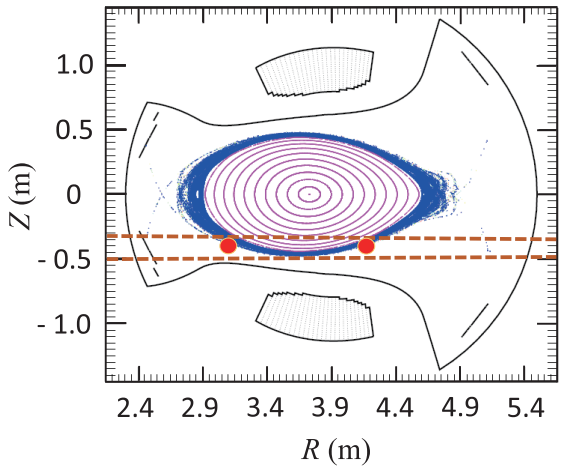

Fig. 4 Schematic drawing of magnetic field surfaces for the plasma axis at $R_{ax} = 3.75$ m along with the observation range covered by the spectrometer (shown with the dashed lines). The $r_{eff} = \pm 0.67$ m locations are shown with circles at $Z = -0.4$ m. Negative and positive values of r_{eff} correspond to the inboard side and the outboard side, respectively.

present case, the direction of the magnetic field is taken as the quantization axis. The results in Sec. 2 correspond to the cases when the angle of observation is 90°. However, in the present experiments in LHD the angle of observation may be different from 90°. Therefore, the results of the theoretical model can not be used directly and the influence of the angle of observation on the final result must be taken into consideration.

3.1 Viewing geometry and calculation of the angle of observation

The hydrogen Lyman-α line has been observed from the edge region of the LHD plasma with a 3 m normal incidence VUV spectrometer [8]. The optical components developed and provided by the CLASP (Chromospheric Lyman-Alpha Spectro-Polarimeter) project [9] team have been additionally installed inside the spectrometer to obtain the polarization-resolved spectra of the Lyman-α line.

Figure 4 illustrates a schematic drawing of the horizontally-elongated cross section of LHD along with the magnetic surfaces for the magnetic axis position at $R_{ax} = 3.75$ m. The field of view is shown with dashed lines. The variables of Z and R are the vertical and the radial coordinates, respectively. According to the previous study, the hydrogen emission is located outside the confined region in LHD and it can be approximated that the emission location is at $r_{eff} = 0.67$ m in the LHD plasma [3,4]. Here, r_{eff} refers to the effective minor radius of the plasma. From this result, it is clear that the Lyman-α is emitted at both the inboard and outboard sides of the device, and the intensity observed by the spectrometer is the sum of these two intensities.

In LHD, the magnetic field is determined accurately by the coil currents. The present discussion focuses on the steady-state time period of an electron cyclotron heated

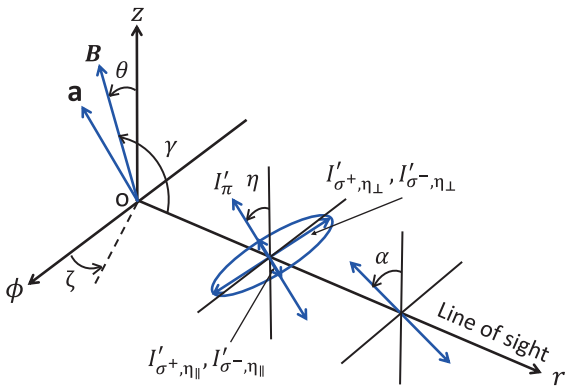

Fig. 5 The definitions of angles of the magnetic field with respect to the line of sight. θ and ζ are the inclination and azimuth angles of the magnetic field vector **B**, respectively. γ is the angle between the line of sight and **B**. **a** is the unit vector in the same direction as the projection of **B** onto the $\phi - z$ plane and η is the angle of **a** with respect to the z axis.

discharge of shot no. 138764. Using the available data, the directions and magnitudes of the magnetic field vectors, **B**, at the emission locations, i.e., $r_{eff} = \pm 0.67$ m have been determined.

Figure 5 shows the angles θ, ζ, and the angle of observation, denoted here as γ. The inclination angle θ represents the angle of the magnetic field **B** with respect to the z direction. The azimuth angle ζ shows the angle between the projection of the magnetic field **B** onto the $\phi - r$ plane and the ϕ direction. The angle of observation γ can be obtained from the inclination angle θ and the azimuth angle ζ using the relation

$$\cos\gamma = \sin\theta \, \sin\zeta. \tag{20}$$

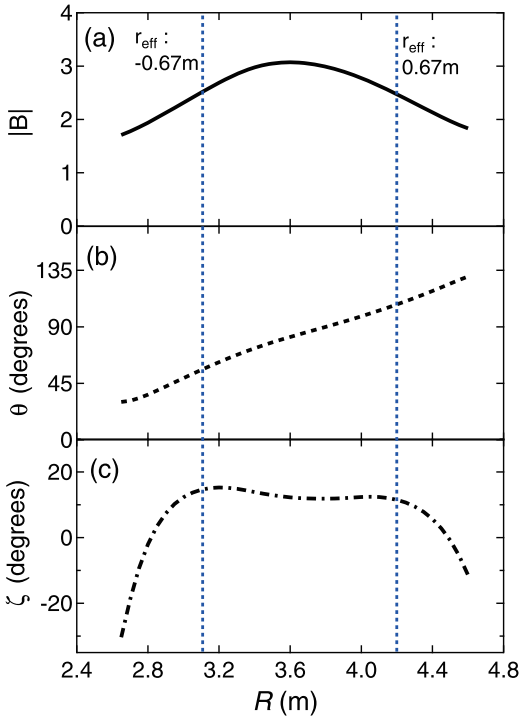

Fig. 6 Magnetic field parameters for shot no. 138764 at $Z = -0.4$ m : (a) the variation of the magnetic field strength, (b) the inclination angle θ of the magnetic field with respect to the z direction, and (c) the azimuth angle ζ which is the angle between the projection of the magnetic field vector onto the $\phi - r$ plane and the ϕ direction. The $r_{\rm eff} = \pm 0.67$ m locations at the inboard side and the outboard side are indicated with the vertical dashed lines.

The **B** vectors point upward and downward at the inboard side and the outboard side, respectively. Although the observation range is 15 cm wide in the Z coordinate, here we consider only $Z = -0.4$ m for simplicity. The parameters of the magnetic field vector **B** at $Z = -0.4$ m are plotted in Figs. 6 (a) - (c). The value of the angle of observation is found to be 77.5° and 79° at the Lyman-α emission locations for the inboard and outboard sides, respectively.

3.2 Derivation of the intensity observed from the line of sight

The Lyman-α line is assumed to be emitted at the position O where the magnetic field **B** is directed as shown in Fig. 5. I_π refers to the linearly polarized light parallel to **B**. I_{σ^+} and I_{σ^-} are the circularly polarized light in the direction perpendicular to **B**. For a particular angle of observation γ, we define a unit vector **a** which is in the same direction as the projection of **B** onto the $\phi - z$ plane. η is the angle of **a** with respect to the z axis.

The π component is observed as the light linearly polarized in the direction of **a**. We denote its intensity as I'_π

$$I'_\pi = I_\pi \sin^2\gamma. \tag{21}$$

The σ^+ component gives rise to the intensities in both the parallel and perpendicular directions to **a**: $I'_{\sigma^+,\eta_\parallel}$ and $I'_{\sigma^+,\eta_\perp}$, respectively.

$$\begin{aligned} I'_{\sigma^+} &= I'_{\sigma^+,\eta_\parallel} + I'_{\sigma^+,\eta_\perp} \\ &= \frac{1}{2}(\cos^2\gamma + 1) I_{\sigma^+}, \end{aligned} \tag{22}$$

and the σ^- component gives rise to the intensities

$$\begin{aligned} I'_{\sigma^-} &= I'_{\sigma^-,\eta_\parallel} + I'_{\sigma^-,\eta_\perp} \\ &= \frac{1}{2}(\cos^2\gamma + 1) I_{\sigma^-}. \end{aligned} \tag{23}$$

In the experiments on LHD, a half-waveplate specially designed for Lyman-α is rotated to monitor the linearly polarized light emission at all angles. Here, we define the angle of the linearly polarized light as the polarization angle, denoted here as α. The intensity observed at the polarization angle α consists of the π component

$$\begin{aligned} I_{o,\pi} &= I'_\pi \cos^2(\eta - \alpha) \\ &= \sin^2\gamma \cos^2(\eta - \alpha) I_\pi, \end{aligned} \tag{24}$$

and the σ^+ and σ^- components

$$\begin{aligned} I_{o,\sigma^+} &= I'_{\sigma^+,\eta_\parallel} \cos^2(\eta - \alpha) + I'_{\sigma^+,\eta_\perp} \sin^2(\eta - \alpha) \\ &= \frac{1}{2}\Big\{ \cos^2\gamma \cos^2(\eta - \alpha) + \sin^2(\eta - \alpha) \Big\} I_{\sigma^+}, \end{aligned} \tag{25}$$

$$\begin{aligned} I_{o,\sigma^-} &= I'_{\sigma^-,\eta_\parallel} \cos^2(\eta - \alpha) + I'_{\sigma^-,\eta_\perp} \sin^2(\eta - \alpha) \\ &= \frac{1}{2}\Big\{ \cos^2\gamma \cos^2(\eta - \alpha) + \sin^2(\eta - \alpha) \Big\} I_{\sigma^-}. \end{aligned} \tag{26}$$

The angle η is related to θ and ζ as

$$\tan\eta = \tan\theta \, \cos\zeta. \tag{27}$$

It should be noted here that the angles θ and η are calculated with respect to the $+z$ axis and the azimuth angle ζ is calculated with respect to the $+\phi$ axis. The total observed intensity at the polarization angle α is given as

$$I_{\rm obs} = I_{{\rm o},\pi} + I_{{\rm o},\sigma^+} + I_{{\rm o},\sigma^-}. \tag{28}$$

We assume axisymmetry with respect to the magnetic field direction. Therefore, in this case $I_{\sigma^+} = I_{\sigma^-} \equiv I_\sigma$. Thus, the final expression for $I_{\rm obs}$ can be given as

$$\begin{aligned} I_{\rm obs} &= \sin^2\gamma \, \cos^2(\eta - \alpha) \, I_\pi \\ &\quad + \Big\{ \cos^2\gamma \, \cos^2(\eta - \alpha) + \sin^2(\eta - \alpha) \Big\} \, I_\sigma. \end{aligned} \tag{29}$$

4. Results and Discussion

4.1 Calculation of polarization for the LHD experiments

The polarization degree, Eq. (16), is defined here with respect to the unit vector **a**. Thus, when in Eq. (29), $\alpha = \eta$, intensity $I_\parallel$ is observed and when $\alpha = \eta + \pi/2$, intensity

$I_\perp$ is observed. The obtained intensities are given by the following equations

$$I_\parallel = I_\pi \sin^2\gamma + I_\sigma \cos^2\gamma, \tag{30}$$

$$I_\perp = I_\sigma. \tag{31}$$

In the present case, the angle of observation is 77.5° and 79° for the inboard and outboard sides, respectively. The electron temperature in this region is roughly 10 eV. The polarization degree has been calculated by assuming $T_\parallel$ = 10 eV and with the angle of observation 77.5°. The result of the calculation is shown in Fig. 7 together with P_{res} obtained for the angle of observation 90°. The perpendicular electron temperature, $T_\perp$, is varied from 3 eV to 30 eV. The results indicate that the polarization values for these two angles of observation are nearly the same. The details of the experimental setup on LHD and of the calculation of polarization degree are given in Ref. [10]. The observed P value is in the order of 0.01, which suggests that the difference between $T_\parallel$ and $T_\perp$ is about 10%.

4.2 Simulation of experimentally observed intensity variation

The derived expression for the intensity observed from the line of sight, Eq. (29), and the obtained values of the angle of observation, γ, can be used to understand the variation of the experimentally monitored intensity with the polarization angle. From such investigation, the information regarding the relation between the magnetic field direction and the intensity profile, and regarding the dominant emission region can be inferred.

The simulated intensity profiles of Lyman-α have been obtained using Eq. (29) and the parameters of the magnetic field at the inboard side and the outboard side. In the present case, we focus on the shot no. 138764 of LHD and the magnetic field values at r_{eff} = ±0.67 m for Z = −0.4 m have been used. These values have been shown in Fig. 6. Positive and negative values of r_{eff} are for the outboard side and the inboard side, respectively. Here the value of polarization degree has been taken to be the same as the experimental value.

Figure 8 shows the variation of the simulated intensities with the polarization angle α for the inboard and outboard sides with the experimentally obtained intensity variation. It is clearly seen that the experimental result agrees with the simulated result for the inboard side. Although the experimental intensity generally consists of emissions from both the inboard and outboard sides, and it is not possible to evaluate local P values at these two sides, this observation suggests that the main contribution to the polarized emission comes from the emission at the inboard side plasma. Even when emission at the outboard side exists, it may be unpolarized and works to lower the observed polarization degree. Due to this reason, although the observed P value is in the order of 0.01, there is a possibility that the local P value at the inboard side may be higher than 0.01 and thus the difference between $T_\parallel$ and $T_\perp$ at the inboard side is larger than 10%.

It is also found that the experimentally obtained intensity is explained only when P is negative. This fact indicates that the electron temperature in the direction perpendicular to the magnetic field is higher than that in the direction parallel to the magnetic field, i.e., $T_\perp > T_\parallel$.

The error in the measured intensity itself is smaller than the symbol size in Fig. 8, and the actual uncertainty of the present measurement is mainly attributed to the unsteadiness of the discharge which is recognized as the discrepancy of the measured intensities from the fitted curve in Fig. 8. For the purpose of estimating the uncertainty of the present measurement, the root mean squared error of the measured intensity with respect to the fitted curve is evaluated and given as the error bars in Fig. 8.

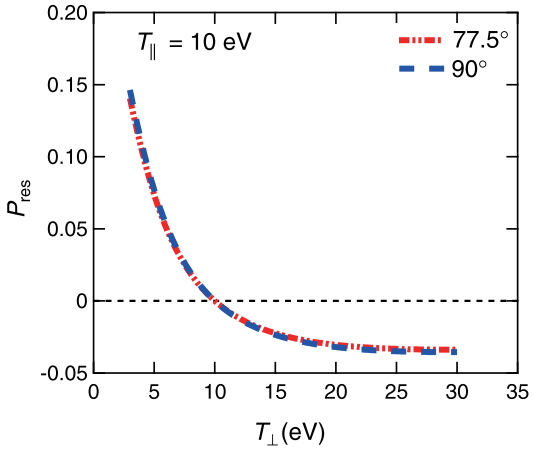

Fig. 7 Polarization degree for the angle of observation 90° (blue dashed line) and 77.5° (red dash-dotted line).

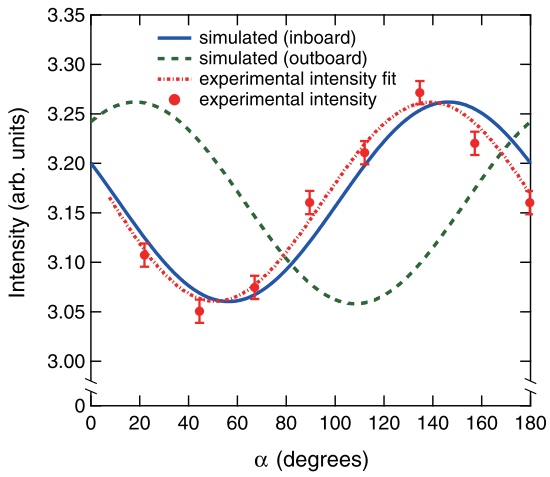

Fig. 8 Lyman-α intensity as a function of polarization angle. The experimental result is plotted with circles and the fitted result is shown with the dashed-dotted line. The solid and dashed lines show the simulated results for the inboard side and the outboard side, respectively.

Acknowledgments

We are grateful to the LHD Experiment Group and the technical staff of LHD for their support of this work. We would also like to thank the CLASP project team for providing the optical components for the LHD experiments. This work is partly supported by JSPS KAKENHI Grant (Number 26287148) and by the National Institute for Fusion Science grant administrative budget (ULHH028).

[1] R. Makino, S. Kubo, T. Ito *et al.*, Plasma Fusion Res. **8**, 2402115 (2013).
[2] T. Fujimoto and A. Iwamae, *Plasma Polarization Spectroscopy* (Springer, Berlin, 2008).
[3] A. Iwamae, A. Sakaue, N. Neshi *et al.*, Phys. Plasmas **17**, 090701 (2010).
[4] A. Iwamae, M. Hayakawa, M. Atake, T. Fujimoto *et al.*, Phys. Plasmas **12**, 042501, (2005).
[5] K. Blum, *Density Matrix Theory and Applications*, 3rd edn. (Springer, Berlin, 2011).
[6] I. Bray and A. Stelbovics, Adv. At. Mol. Opt. Phys. **35**, 209 (1995).
[7] G.K. James, J.A. Slevin, D. Dziczek, J.W. McConkey and I. Bray, Phys. Rev. A **57**, 1787 (1998).
[8] T. Oishi, S. Morita *et al.*, Appl. Opt. **53**, 29 (2014).
[9] R. Kano, T.J. Bueno, A. Winebarger *et al.*, Astrophys. J. Lett. **750**, L11 (2017).
[10] N. Ramaiya, M. Goto, T. Oishi and S. Morita, to be published in J. Phys.: Conf. Ser.